# We are IntechOpen, the world's leading publisher of Open Access books Built by scientists, for scientists

6,900
Open access books available

185,000
International authors and editors

200M
Downloads

Our authors are among the

154
Countries delivered to

TOP 1%
most cited scientists

12.2%
Contributors from top 500 universities




WEB OF SCIENCE™

Selection of our books indexed in the Book Citation Index in Web of Science™ Core Collection (BKCI)

## Interested in publishing with us?
## Contact book.department@intechopen.com

Numbers displayed above are based on latest data collected.
For more information visit www.intechopen.com



Chapter 13

# Spin-Coating Technique for Fabricating Nickel Zinc Nanoferrite ($Ni_{0.3}Zn_{0.7}Fe_2O_4$) Thin Films

Yusnita Yusuf, Raba'ah Syahidah Azis and Muhammad Syazwan Mustaffa

Additional information is available at the end of the chapter

http://dx.doi.org/10.5772/intechopen.80461

**Abstract**

Functional nanoferrite thin films are used in various fields of our life. There are many different methods used to fabricate thin films including sputter deposition, flash laser evaporation pulsed laser deposition (PLD), chemical vapor deposition (PVD) and spin-coating process. In each of these methods, it produces an amorphous phase of the deposited film. To produce a crystalline film, an additional high-temperature processing is required. The high-temperature process can lead to considerable constraints in combining the desirable characteristics of a crystalline nanoferrite thin film with those of thermally unstable substrates and other device components. High-temperature thin-film processing is also a considerable cost to manufacturing. This chapter will report a simple procedure of the sol-gel precursor method for fabrication of NiZn nanoferrite ($Ni_{0.3}Zn_{0.7}Fe_2O_4$) thin films and spin-coating method in coating a chemical solution. This method generally provides for both low-temperature deposition and crystallization of NiZn nanoferrite thin films.

**Keywords:** NiZn ferrite thin films, spin coating, structural, magnetic, optical properties

## 1. Introduction of NiZn ferrite thin films

NiZn nanocrystalline ferrite thin films have a spinel crystal structure which have been a subject of extensive attempt because of their potential applications in high-density magneto-optic recording devices, magnetic refrigeration and microwave materials due to its high electrical resistivity, low magnetic coercivity and low eddy current losses. NiZn nanoferrite thin films are structure sensitive, and it is not easy to produce a stoichiometric and point-defect-free NiZn ferrite, for high-resistivity applications**.** In NiZn ferrite thin-film fabrication, the

IntechOpen

© 2018 The Author(s). Licensee IntechOpen. This chapter is distributed under the terms of the Creative Commons Attribution License (http://creativecommons.org/licenses/by/3.0), which permits unrestricted use, distribution, and reproduction in any medium, provided the original work is properly cited. CC BY

accurate composition control and the uniformity throughout the film deposition are important. It is well known that properties of ferrite materials strongly depend on the preparation conditions. This issue is important in NiZn ferrite thin films because the effect of temperatures will lead to the change in the chemical composition of the ferrite films. These also will result in non-uniformity of film composition and the magnetic hysteresis parameter of ferrites. High-temperature synthesis of NiZn thin-film ferrite results in the evaporation of some constituents that lead to the nonstoichiometry, and zinc volatilization at higher temperature can result in the formation of $Fe^{2+}$ ions that lead to increase the electron hopping and reducing the electrical resistivity [1]. Therefore, a low-temperature synthesis is required for the synthesis of NiZn ferrite film. Properties of ferrite film depend on the preparation route, due to its strong influence on type of the film (polycrystalline and epitaxial), particle size, chemical homogeneity, microstructure and cationic distribution between tetrahedral and octahedral sublattice sites [2, 3]. Synthesis of ferrite thin film is of great interest among researchers in this field of study. Widely used techniques are utilized to produce desirable final product of nickel zinc ferrite. These techniques can be classified into two major techniques which are the conventional technique and the nonconventional technique. The starting materials are conventionally oxides or precursors of oxide of the cations. This process involves the interdiffusion of the various metal ions of preselected compositions to form a mixed crystal. The nonconventional powder processing in a liquid medium may produce intermediate, finely divided mixed hydroxides or mixed organic salts to assist the subsequent diffusion process [4]. Most of ferrite films have been prepared using sputtering and pulsed laser deposition. Somehow, sol-gel method is a kind of potential film preparation process, which possesses advantages of chemical homogeneity, easy component adjustment, low calcination temperature and low cost. Spin coating gives an advantage to liquid film that leads to uniformity in thickness during spin-off [5]. Once uniform, it tends to remain provided the viscosity is not shear-dependent and does not vary over the substrate. Other than that, sol-gel and hydrothermal routes of ferrite synthesis have shown increasing importance. Recent years are marked by growing interest in sol-gel processed films in new areas, particularly in microelectronics. This is mainly due to intensively developing applications of silicate or siloxane sol-gel films in the VLSI multilevel interconnection process, the preparation of ferroelectric films for nonvolatile memory [6].

## 2. Literature review on synthesis techniques of NiZn ferrite thin films

Spin coating is widely used in modern optical and microelectronic industries [7]. The understanding of its underlying physics remains limited, a fact attributed to the lack of experimental data for the evolution of various parameters during the process [8, 9], leading to the need for new evolution tools. A relative study of nickel zinc ferrite by sol-gel route and conventional solid-state reaction was carried out [10]. It was claimed that the homogeneity and high purity in the sol-gel samples and small grains confirmed the finer particles. $Ni_{0.36}Zn_{0.64}Fe_2O_4$ (NZF) thick films have been synthesized using sol-gel dip-coating method [11]. Combination with dispersion of ceramic NZF particles in starting sols has been proved to be useful for producing thick nickel zinc ferrite films. The best NZF powders are formed from dispersing at 300°C by

hydrothermal grow. Nickel zinc ferrite thin films are successfully prepared using spin-deposited citrate-precursor route [12]. The formation of crystalline film at low temperature even though films were found to be X-ray amorphous revealed the formation of uniform grains in nanometer size range. Besides that, NiZn ferrite film was successfully fabricated by using photosensitive sol-gel method. The photosensitive gel film can be the photoresist of itself during the preparation process. The fine pattern of $Ni_{0.5}Zn_{0.5}Fe_2O_4$ film is obtained through UV radiation, rising and heat treatment [13]. The great potential of combining the microwave technique with nonaqueous sol-gel chemistry was successful [14]. Many transition metal ferrite nanoparticles with high crystallinity are uniformly morphological besides homogenous metal ferrite thin films on flat and curved substrates. The thickness of film can easily be adjusted in the range of 20–80 nm using precursor concentration. Other synthesis techniques of nickel zinc ferrite thin films are chemical vapor deposition, spray pyrolysis, sputtering, pulsed laser deposition and spin spray. Of these methods the earliest used was vapor deposition of metals followed by oxidation [15]. The films were porous and polycrystalline and approximately 1000 Å thick. Many common ferrites produced by this method were single-phase spinel in crystal structure. Spray pyrolysis is complicated and expensive and required special equipment and sometimes high processing temperature above 500°C. By using spray pyrolysis technique [3, 16], very homogenous ferrite thin films were obtained with good reproducibility. Nevertheless, for spinel ferrite thin-film growth, this method is used rarely. Also only a few works can be found on NiZn ferrites, obtained by spray pyrolysis where a focus on the investigation of microstructural, optical and magnetic properties was held [17]. Apart from that, the effect of oxygen plasma treatment on magnetic and NiZn ferrite films using the spin-spray plating method has been employed [18]. The oxygen plasma treatment increased the number of nucleation sites of ferrite and enhanced adhesion of the films to the substrates. It has been reported that spinel Zn ferrite can be synthesized without substrate heating by pulsed laser deposition [19]. However, this technique needs post-deposition and requires sputtered film at a high temperature to grow the spinel ferrite structure. The results were optimized and obtained 4000 Å NiZn ferrite films with low in-plane coercivity of $H_c$ = 15.2 Oe and relatively high saturation magnetization $M_s$ = 318 emu/cm$^3$. Some other research works was working on preparing NiZn ferrite films by magnetron sputtering method. Most of the sputtered ferrite films must be deposited at a high substrate temperature and need high heat treatment to obtain ordered spinel structure. Sputtering method is prepared at room temperature without any post-annealing treatment [20]. By controlling the relative oxygen flow, grain size in a range 10–20 nm was developed. It revealed a maximum saturation magnetization of about 151 emu/cm$^3$. The static magnetic measurement results are affected by the crystallinity, grain dimension and cation distribution.

## 3. Brief overview of preparation methods

### 3.1. Preparation of NiZn ferrite thin films

NiZn ferrite thin film is prepared by a sol-gel process and spin-coating technique. The starting materials nickel nitrate hexahydrate ($Ni(NO_3)_2 \cdot 6H_2O$) (Sigma Aldrich, 99.999%), iron nitrate nonahydrate ($Fe(NO_3)_3 \cdot 9H_2O$) (Alfa Aesar, 99.999%) and zinc nitrate hexahydrate

($Zn(NO_3)_2 \cdot 6H_2O$) (Alfa Aesar, 99.999%) with high purity were used as a precursor for the starting sol preparation. The materials are in metal nitrate hydrates which are soluble in alcohol solvents. Acetone and deionized water were used as a medium for sol-gel reaction. Acetic acid ($C_6H_8O_7H_2O$) (Alfa Aesar, 99.99%) acts as the chelating agent. The precursors were dissolved in deionized water and stirred for 15 min with a molar ratio of Ni:Zn:Fe = 1:1:2 using hot plate. The former salt solution was dissolved into acetic acid solution with a molar ratio of 1:1 and stirred for 3 h at 80°C. A sol-gel formed was left 24 h for age.

### 3.2. Thin film deposition and spin-coating technique

The thin film was deposited on indium tin oxide (ITO) glass. ITO has higher melting point around 1926°C. There is no phase change of substrate during deposition of the film. The typical properties of ITO glass substrate are listed in **Table 1**. The film deposition consists of substrate wash and spin coating. The steps are to wash the substrates firstly with distilled water in ultrasonic bath for 15 min. The substrate was then washed in ultrasonic bath using acetone liquid for 15 min. Coating was carried out in a clean room by using a spin coater. The setting parameters were listed in **Table 2**. The aged sol of 1.0 ml (Section 3.1) was dropped on ITO glass substrate and spin coated for 25 s at 3500 rpm (revolutions per min). The deposition was repeated several times to obtain the required thickness (300 nm). The film thickness can be controlled by the number of coating. The film with desired thickness can be obtained by repeating the deposition cycle. Then drying films were performed in a room temperature for a few minutes and annealed in air at temperature 400, 500, 600 and 700°C, respectively, with an increment of 100°C for 1 h. Annealing process was performed in a box furnace with rate of 5°C/min.

### 3.3. $Ni_{0.3}Zn_{0.7}Fe_2O_4$ thin-film characterizations

The X-ray diffraction (XRD) pattern of $Ni_{0.3}Zn_{0.7}Fe_2O_4$ thin films was obtained by using a Philips X'pert diffractometer model 7602 EA Almelo operating at 40 kV/30 mA in the 2θ range (20–80°) with CuKα radiation, λ = 1.5418 Å. The microstructural properties were

| | |
|---|---|
| Glass substrate | ITO coating glass |
| Size of substrate | 25 × 12 × 1.1 mm |
| Gel drop | 1 ml |
| Wash ultrasonic bath | 15 min |
| Spin rotations per min (rpm) | 3500 |
| Duration of cycle | 25 s |
| Number of cycle | 5 |
| Annealing temperature | 400–700°C |
| Cooling rate after annealing | 5°C/min |

**Table 1.** Experimental parameters of $Ni_{0.3}Zn_{0.7}Fe_2O_4$ thin-film sol-gel spin-coating deposition process.

| | |
|---|---|
| Speed rate (rpm) | 3500 rpm (constant speed) |
| Spin time (s) | 25 s |
| Volume of solution | 1.0 ml |
| Acceleration and deceleration | 140 rpm/s |
| Temperature | Room temperature |

Reproduced with permission from [21].

**Table 2.** Spin-coating setting parameters.

observed using a FEI Nova NanoSEM 230 field emission scanning electron microscope. The distributions of grain sizes were obtained by taking more than 200 different grain images for the sample using J-image software. Hysteresis parameters of the loop of the $Ni_{0.3}Zn_{0.7}Fe_2O_4$ thin films were measured by using vibrating sample magnetometer (VSM) model 7404 Lake Shore. UV-Vis SHIMADZU model UV-3600 spectrophotometer has been used to analyse the optical transmission of the NiZn ferrite thin film in the wavelength range 200–800 nm.

## 4. Research findings

### 4.1. Structural analysis

**Figure 1** shows the XRD pattern of spin coating and air-annealed ferrite thin films on the ITO glass substrate. The XRD patterns show single-cubic spinel-phase structures of (220), (311), (400), (511) and (440) in $Ni_{0.3}Zn_{0.7}Fe_2O_4$ ferrite thin films according to JCPDS reference code 74-2081 and 82-1049, respectively. Plane (311) is most intense in each annealing temperature, whereas others are at relatively low intensity [22]. These plane formed nickel zinc ferrite phases. The small peak intensities in XRD pattern revealed the existence of fine grain nanocrystalline with the most part as amorphous. The height of the highest XRD intensity is more intense at high temperature and improves the crystallinity of the films. As the annealing temperature increases, the grain size also increases, as indicated in the narrowing of the XRD spectrum lines. Increasing annealing temperature will enhance the crystallinity besides releasing the internal strains within the samples which results in better optical and magnetic properties. The intensity of the (311) peak increases as a function of the substrate temperature showing an improvement of the film crystallinity. Moreover the peak intensity increases, while its full width at half maximum (FWHM) decreases. Further increasing of substrate temperature leads to a slight decrease of the peak intensity for films prepared at 700°C. It indicates a saturation of film crystallinity. The crystallite sizes of all ferrite thin films are found to be between 16 and 18 nm. The average crystallite size, $D$ (**Table 4**), was determined using the Scherrer's formula [23] as given by Eq. (1):

$$D = \frac{0.9\lambda}{\beta \cos\theta} \tag{1}$$

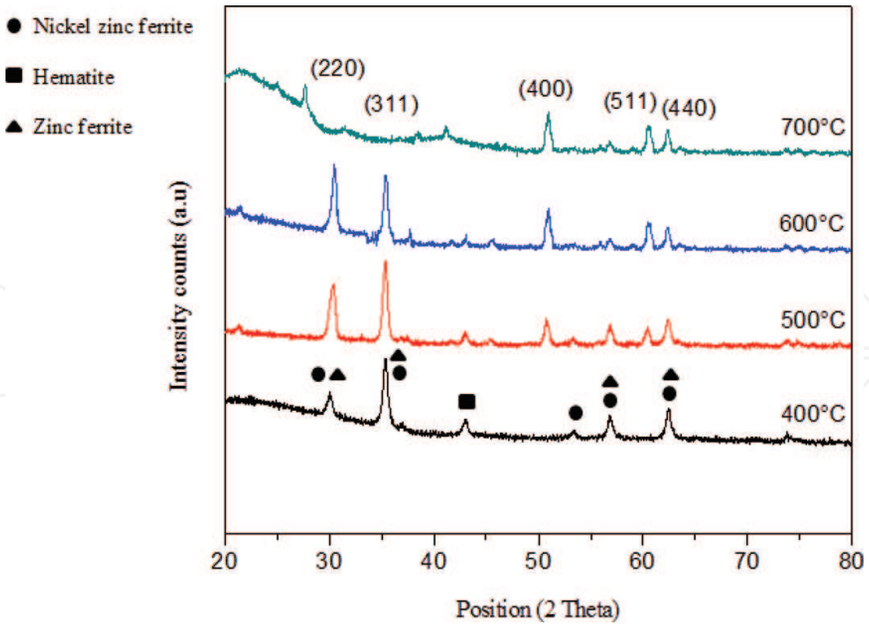



**Figure 1.** XRD pattern of air-annealed $Ni_{0.3}Zn_{0.7}Fe_2O_4$ ferrite thin films. Reproduced with permission from [21].

where $D$ is the crystallite size, $\beta$ is full width at half maximum of the diffraction peak, $\lambda$ is the wavelength of 1.54 Å, and $\theta$ is scanning angle.

The lattice constants of these films were calculated using indexing method [24] given by Eq. (2):

$$\frac{\lambda}{4\,a^2} = \frac{\sin^2\theta}{d} = \frac{\sin^2\theta}{(h^2+k^2+l^2)} \tag{2}$$

where $d$ is interplanar spacing, $\lambda$ is X-ray wavelength, and $\theta$ is reflection angle. The $\lambda/4a^2$ is a constant and $d = h^2 + k^2 + l^2$, which is determined by $\sin^2\theta$ value.

These lattice constants are tabulated in **Table 3**. The lattice parameters of all the ferrite films do not match precisely with the standard JCPDS bulk values which could be attributed to the strains present on the surface of the films during the synthesis [25, 26]. Annealing temperature has a pronounced effect on grain size. The lattice parameter calculated for nickel ferrite thin film is 8.338 Å [27]. This is in accordance with the variation in lattice parameter with Zn content reported for the bulk ferrites.

### 4.2. Microstructure analysis

The FESEM images revealed that the $Ni_{0.3}Zn_{0.7}Fe_2O_4$ films have dense and homogenous grains with an average grain size. Film annealed at 400°C was homogenous with dense microstructure, and they have high adhesion to the substrate. Film annealed at 500°C shows a well-developed grain. The grains slowly appeared with increasing annealed temperature. This is because the grain tends to combine with closer grain to form larger grain size. The structure formed in the thin films is a normal characteristic of film derived from sol-gel. The average grain sizes of the $Ni_{0.3}Zn_{0.7}Fe_2O_4$ nanoferrite thin films are 18.61 nm (400°C), 26.25 nm (500°C),

| Annealing temperature (°C) | 400 | 500 | 600 | 700 |
|---|---|---|---|---|
| Rel. intensity counts (%) | 100 | 100 | 100 | 100 |
| Position (2θ) | 35.3661 | 35.3717 | 35.3991 | 35.3247 |
| FWHM (2θ) | 0.5215 | 0.5371 | 0.5116 | 0.4723 |
| *d*-spacing (nm) | 2.53595 | 2.53557 | 2.53207 | 2.53993 |
| Crystallite size (nm) | 16.71 | 16.22 | 17.03 | 18.45 |
| Lattice strain (%) | 0.71 | 0.73 | 0.70 | 0.65 |
| Space group | *F d 3 m* | *F d 3 m* | *F d 3 m* | *F d 3 m* |
| Lattice parameter $a = b = c$ (Å) | 8.4030 | 8.4030 | 8.4030 | 8.4030 |
| Volume/Å$^3$ | 593.34 | 593.34 | 593.34 | 593.34 |

**Table 3.** Structural parameters of $Ni_{0.3}Zn_{0.7}Fe_2O_4$ thin films from XRD spectra.

28.12 nm (600°C) and 41.32 nm (700°C). The grains of the films are spherical and uniform, and cohesion of grains is due to the magnetic attraction. The average grain size of the films is presented in **Figure 2**. The histogram of grain size distribution shifted to the larger grain size as the annealing temperature increased. However, based on the coercivity, $H_c$ results (Section 4.3), the transition from 600 to 700°C of annealing temperature exhibits a fall of the $H_c$ value.

**Figure 3** illustrates the cross section of the samples annealed at 400, 500, 600 and 700°C, respectively. The deposited films were uniform with two cycles of number deposition cycle. It was found that the thin films have thickness in the range of 145.7–285.6 nm which was confirmed by cross-sectional FESEM images. The grain size over 26 nm was further increased with a higher annealing temperature. Accordingly, the number of grain sizes beyond the single domain to multidomain critical size also increased. Therefore, the number of domain wall increased as the movement of domain wall contribution to make ease of magnetization increased [28].

**Figure 4** presented the thickness of the $Ni_{0.7}Zn_{0.3}Fe_2O$ ferrite thin films and shows its relationship with the grain size. Annealing is a process related to secondary grain growth in the film. Thompson discussed the secondary grain growth mechanism and came to the conclusion that the secondary grain growth is driven by the reduction of the total grain boundary energy. Since the grain boundary energy is film-thickness-dependent, the secondary grain growth rate increases when the film thickness is reduced [29].

### 4.3. Magnetic properties

The plots of magnetization, *M*, against magnetic field strength, *H* (*M*–*H* hysteresis loop), for $Ni_{0.3}Zn_{0.7}Fe_2O_4$ films annealed at 400, 500, 600 and 700°C were shown in **Figure 5**. The hysteresis shape is narrow and has linear loops which have a low saturation magnetization, $M_s$. The saturation magnetization, $M_s$, and coercivity, $H_c$, values have been directly extracted from these curves and have been listed for various annealing temperatures in **Table 4**. The $M_s$ and $H_c$ could be attributed to the varied grain size and crystallinity. The lower value of saturation

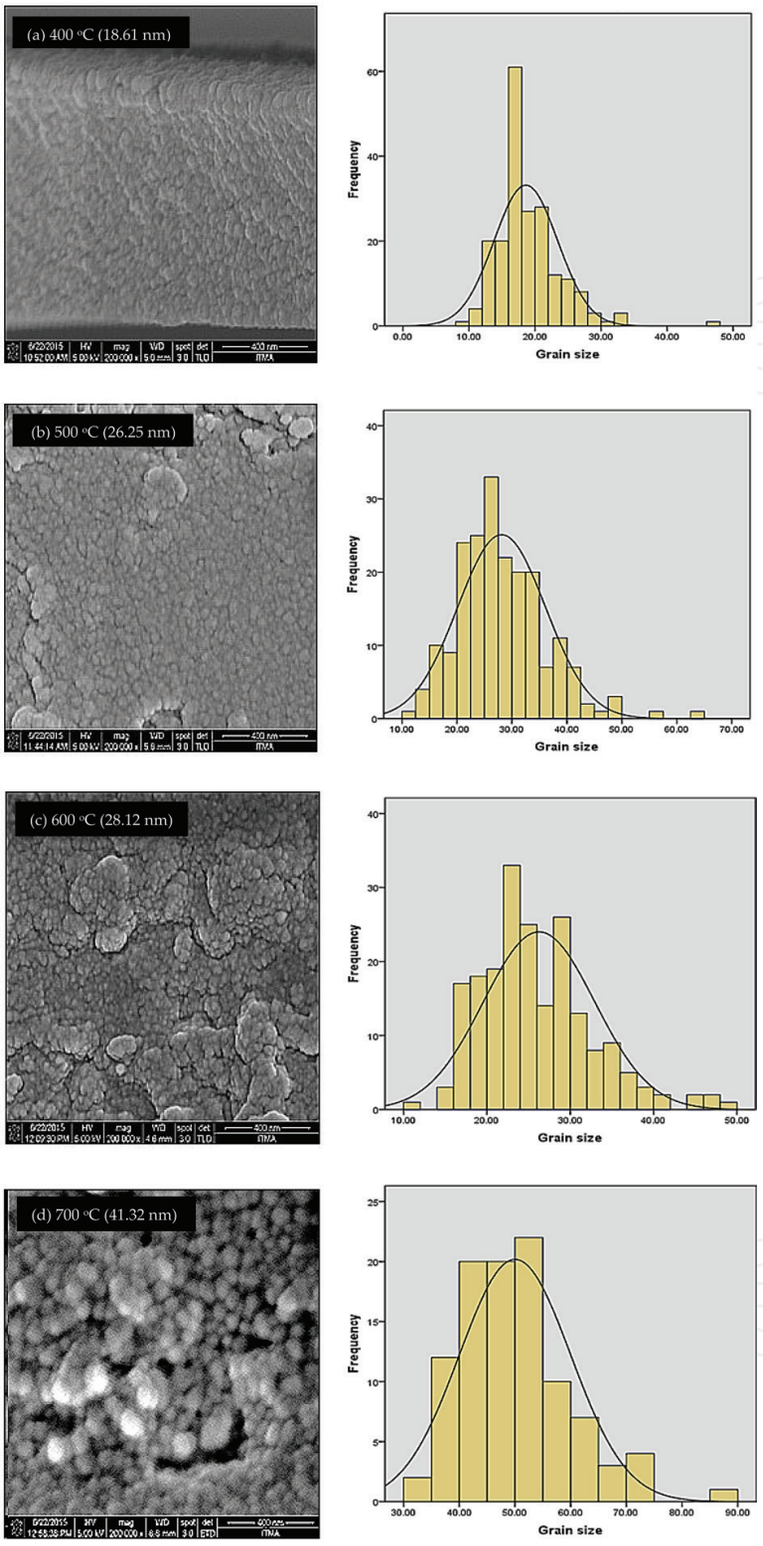



**Figure 2.** FESEM images of the $Ni_{0.3}Zn_{0.7}Fe_2O$ nanoferrite films annealed at (a) 400, (b) 500, (c) 600 and (d) 700°C. Reproduced with permission from [21].

magnetization, $M_s$, $Ni_{0.3}Zn_{0.7}Fe_2O_4$ films (**Figure 6(a)**) could be caused by several reasons. A large grain boundary volume presented in thin films would result in the increase of the $M_s$ [30]. Other reasons for the increase $M_s$ are due to complex spinel structure; it was difficult to gain

http://dx.doi.org/10.5772/intechopen.80461

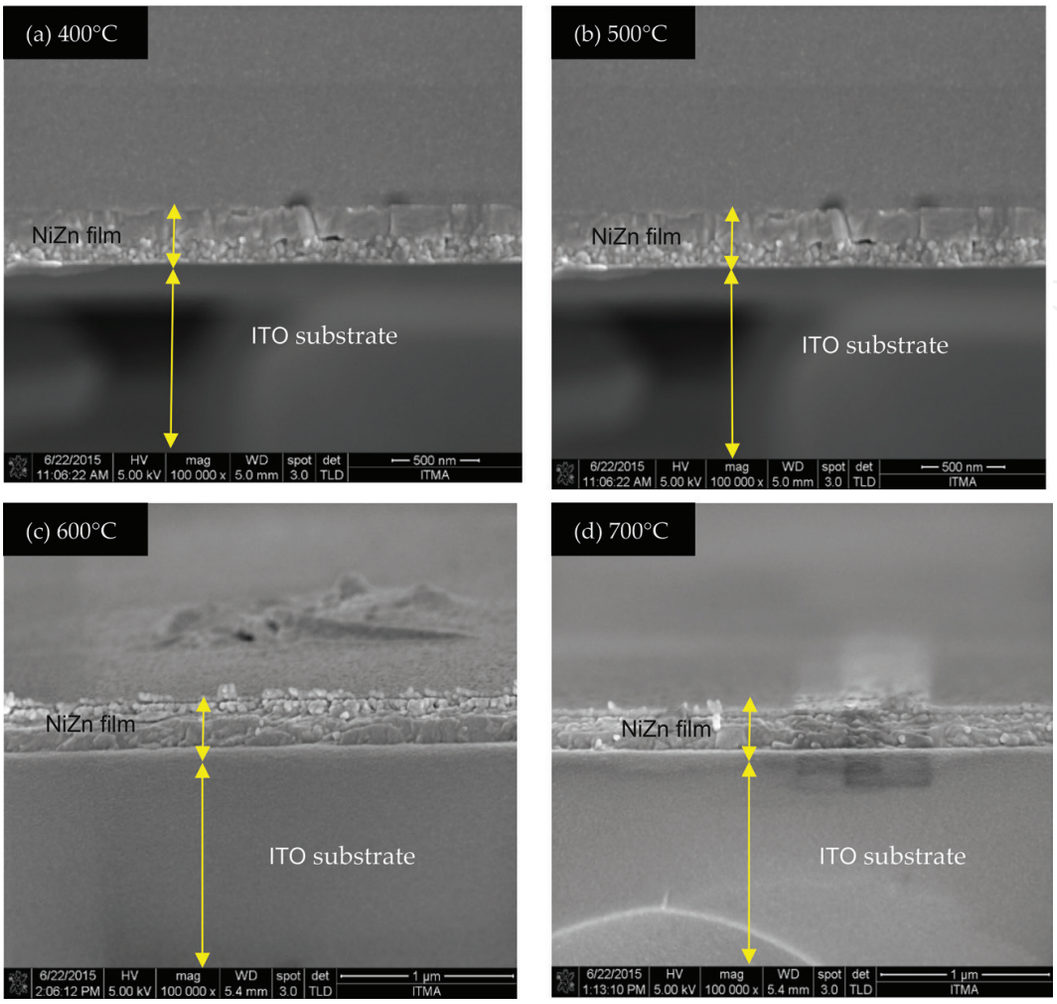



**Figure 3.** Cross-sectional of $Ni_{0.3}Zn_{0.7}Fe_2O$ nanoferrite films annealed at different temperatures.

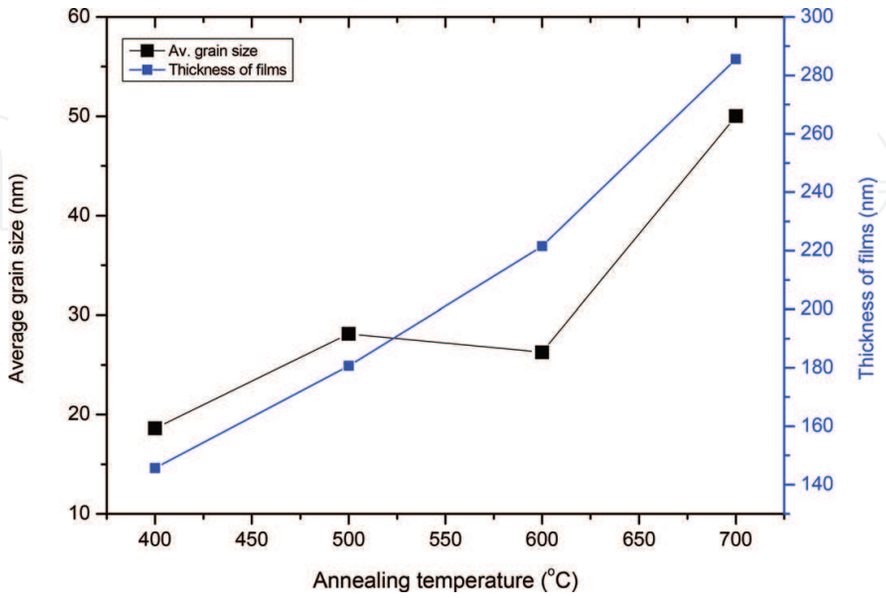



**Figure 4.** The average grain size and film thickness as a function of annealed temperatures. Reproduced with permission from [21].

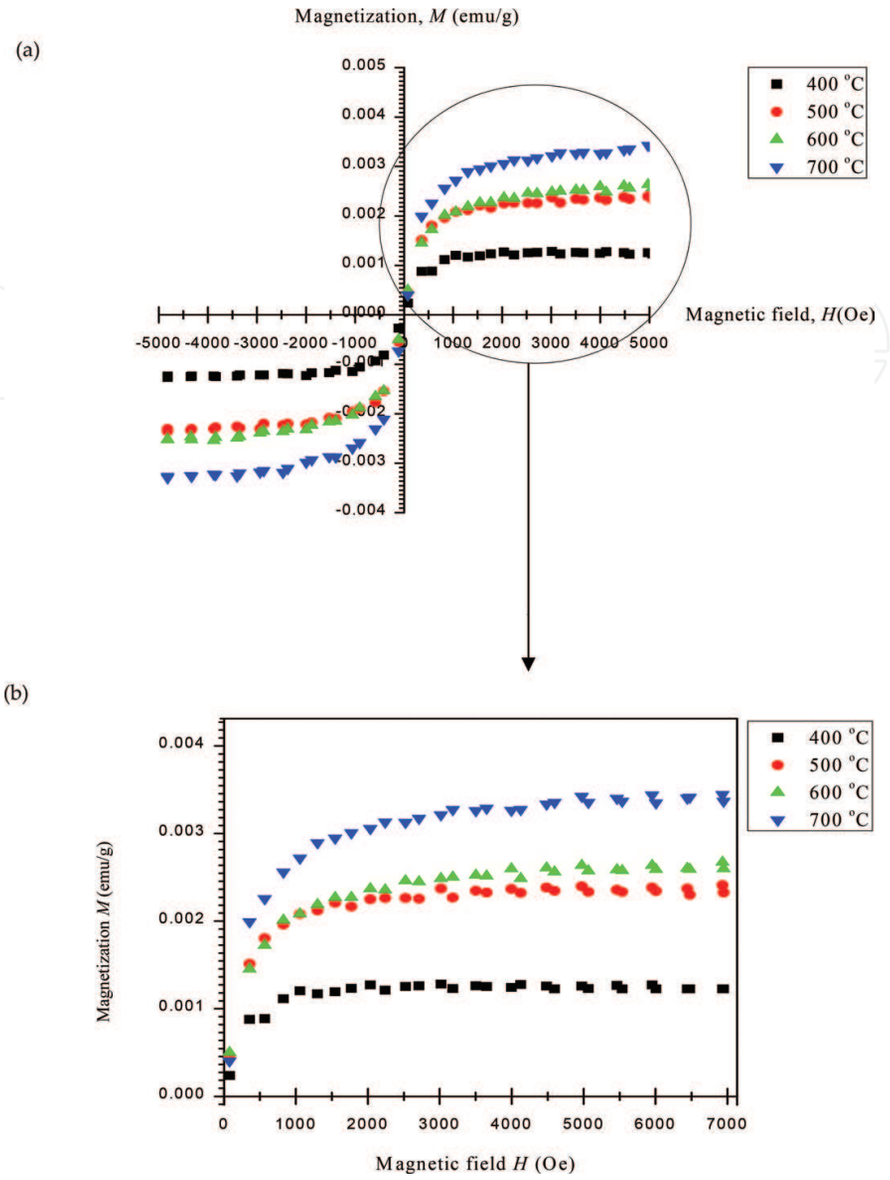



**Figure 5.** (a) Hysteresis loop of $Ni_{0.7}Zn_{0.3}Fe_2O$ ferrite thin films and (b) first quadrant of the magnetic hysteresis loops of the samples. Magnetization at any given field increased with heat treatment temperature. Reproduced with permission from [21].

| Temperature (°C) | $M_s$ (±0.01 emu/g) | $H_c$ (±0.001 Oe) | $D$ (±0.1 nm) | $d_{xrd}$ (±0.01 nm) |
|---|---|---|---|---|
| 400 | 1.287 | 16.184 | 18.6 | 16.71 |
| 500 | 2.395 | 16.536 | 26.3 | 16.22 |
| 600 | 2.653 | 12.288 | 28.1 | 17.03 |
| 700 | 3.421 | 8.297 | 42.32 | 18.45 |

Reproduced with permission from [21].

**Table 4.** Saturation magnetization, $M_s$, coercivity, $H_c$, grain size, $D$, and calculated crystallite size from XRD $d_{xrd}$ of $Ni_{0.3}Zn_{0.7}Fe_2O_4$ nanoferrite thin films.

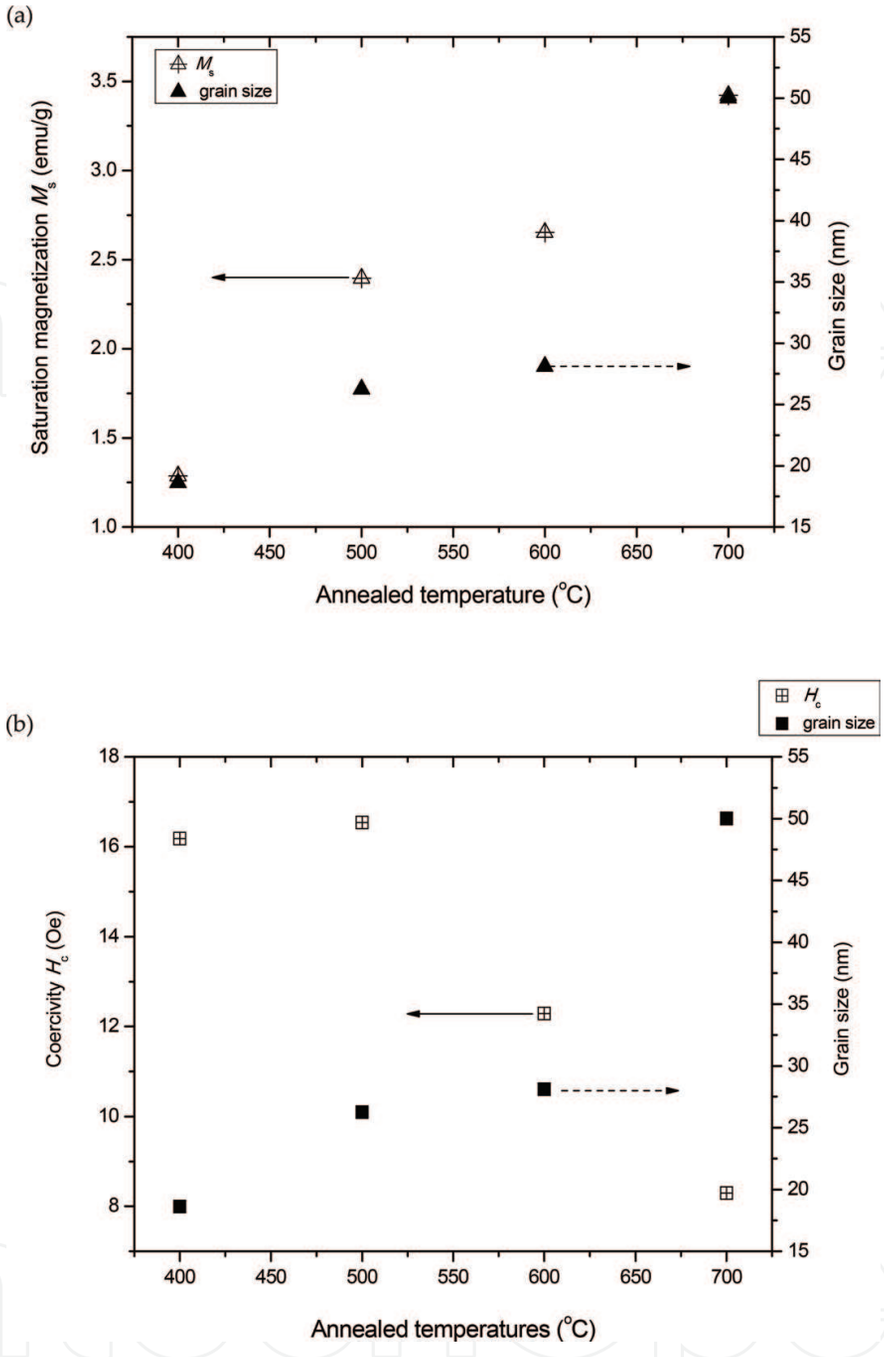



**Figure 6.** Comparison of the variation in (a) $M_s$ and (b) $H_c$ as a function of annealed temperatures of the $Ni_{0.3}Zn_{0.7}Fe_2O$ nanoferrite thin films. Reproduced with permission from [21].

$Ni_{0.3}Zn_{0.7}Fe_2O$ nanoferrite films with perfect crystallization. The metal cations can occupy either *A* sites (tetrahedral) or *B* sites (octahedral), which will result in a partially disordered cation distribution in the crystal lattice [31]. The saturation magnetization ($M_s$) increases with the grain size, and the observations on larger decrease are interpreted mostly by oxygen absorption, characteristic to the preparation technique. The coercivity, $H_c$, was decreased as the annealing temperature and average grain size increased (**Figure 6(b)**). The maximum value of $H_c$ was 16.54 Oe for the grain size 26.25 nm. The $H_c$ observed were closed to the reported value of $H_c$ which is

within the range of 20–210 Oe [20]. The decreases of $H_c$ were contributed from the transition of the single domain to the multidomain [32]. The coercivity ($H_c$) has a maximum grain size of about 26 nm and a steep decrease at larger grain sizes (41.3 nm). The smaller grain sizes and the decrease of $H_c$ are due to the randomizing effects of thermal energy. Thermal energy has an important role in magnetic instability of single-domain magnetic particles. Due to the smaller grain sizes, the thermal agitation becomes small and will not be able to cause fluctuations in the magnetic spin orientations of the nanoparticles where they freeze in random orientations. The latter is probably due to the decreased anisotropy constant, which leads to a sharp decrease in coercivity according to the random anisotropy model. The relation between the decrease $H_c$ and

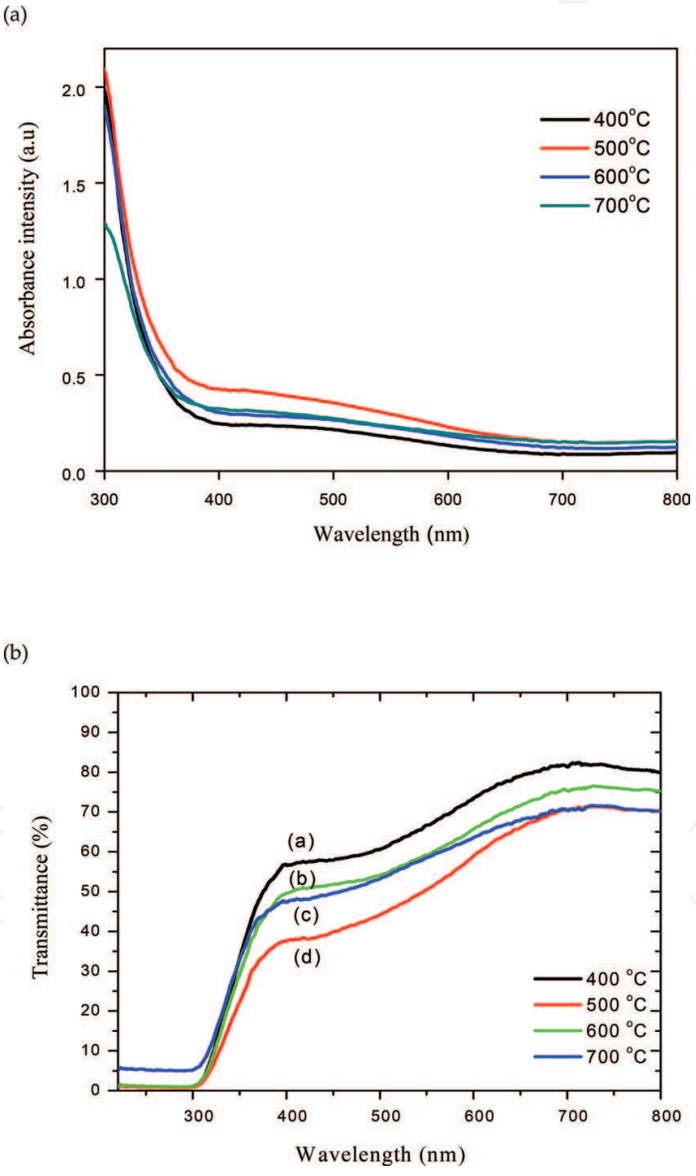



**Figure 7.** (a) Absorbance spectra of thin film at various annealed temperatures and (b) transmittance spectra of NiZn ferrite thin films.

increase grain size shows the linear inverse proportionality between coercivity, $H_c$, and grain size, $D$, by $H_c \alpha 1/D$ [22, 33].

### 4.4. Optical properties

**Figure 7** demonstrates the curves of absorbance and transmittance, respectively. The absorption spectrum exhibits that NiZn ferrite thin films have low absorbance in visible region and it is close to infrared region (**Figure 7(a)**). However, absorbance in UV region is high. This result of the optical behaviour is analogous to those claimed by [34] or cobalt ferrite thin film using microwave-assisted nonaqueous sol-gel process. Optical transmittance is plotted in a wavelength range of 200–800 nm as shown in **Figure 7(b)**. The films are highly transparent in the visible range below 90%. The average transmittance is calculated and tabulated in **Table 5**. The optical transmittance spectra of annealed thin films show a good transmission in the visible region and a sharp fall in the UV region which corresponds to the band gap. The decrease of the transmittance is due to the interaction of the incident long-wavelength radiation with the free electron in the films [35].

**Figure 8(a)** and (**b)** demonstrates the optical band-gap energy direct and indirect of the films annealed at various temperatures. The band-gap energy ($E_g$) of the thin films was calculated from UV–Vis absorbance spectra. Direct and indirect band-gap energies can be obtained from the dependencies $(\alpha hv)^2$ on $hv$, where $\alpha$ is the absorption coefficient, whereas $hv$ is the photon energy in eV [36]. A linear line was obtained by plotting $(\alpha hv)^{1/n}$ against $hv$. The intersection of this straight line on $x$-axis gives the value of optical band gap. The values of band gap as listed in **Table 5** do change with thickness. A dependence of band-gap energy shift on the grain size is attributed to electron confinement effect related with the grain size in the films. As a result, the observed decrease in $E_g$ with increasing grain size is due to the decrease of resistivity and the increase of film thickness. It has been studied that the band gap does not change significantly with the thickness after the film grows completely [37]. The band gap becomes saturated for a particular value of thickness [38]. The presented values of optical band-gap energy are larger than reported value for NiZn ferrite film 1.66 eV [39] and bulk NiZn ferrite, 1.55–1.66 eV [40]. The direct and indirect band energy increases could be the effect of strain present in the films during heat treatment [41].

| Annealing temperature (°C) | Thickness (nm) (±0.1 nm) | Direct band-gap energy $(\alpha hv)^2$ (±0.01 eV) | Indirect band-gap energy $(\alpha hv)^{-1/2}$ (±0.01 eV) | Average transmittance (T%) (±0.1%) | Grain size (±0.01 nm) |
|---|---|---|---|---|---|
| 400 | 145.7 | 3.76 | 3.03 | 85.0 | 18.61 |
| 500 | 180.7 | 3.66 | 3.08 | 78.0 | 26.25 |
| 600 | 221.5 | 3.58 | 3.16 | 70.0 | 28.12 |
| 700 | 285.6 | 3.04 | 3.30 | 70.0 | 41.32 |

**Table 5.** Thickness, band gap, transmittance and grain size of sample at various annealing temperatures.

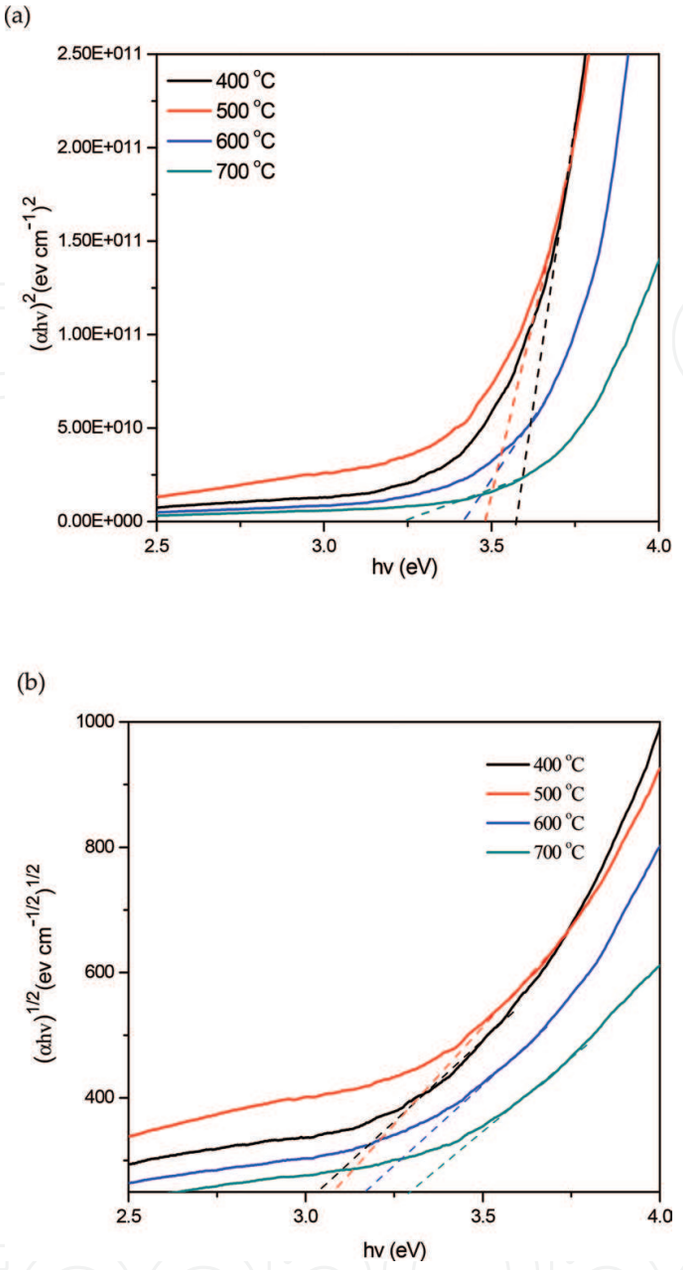



**Figure 8.** (a) Plot of $(\alpha hv)^2$ as a function of photon energy (eV) and (b) Plot of $(\alpha hv)^{1/2}$ as a function of photon energy (hv).

## 5. Summary

NiZn ferrite thin film with composition $Ni_{0.3}Zn_{0.7}Fe_2O_4$ was successfully prepared using sol-gel spin-coating technique. The structure formed in the thin films is a normal characteristic of film derived from sol-gel. Sol-gel spin-coating method was able to produce the similar trend and behaviour, among others, of ferrite thin film. The results are summarized as follows:

- The phase analysis of films produced the complete phase with the formation of spinel structures of $Ni_{0.3}Zn_{0.7}Fe_2O_4$ ferrite which were observable at annealed 400°C and upwards.

Further annealing temperature demonstrated the improvement in the degree of crystallinity of the annealed films.

- The saturation magnetization, $M_s$, of the synthesized $Ni_{0.3}Zn_{0.7}Fe_2O_4$ ferrite thin films has been obtained at room temperature from the hysteresis loops which increases with annealing temperatures. The hysteresis shape shown is narrow and has linear loops which have a low $M_s$. The coercivity, $H_c$, decreases as the average grain size increases since the alignment of the magnetic moments inside the domain is fully controlled by thermal energy.
- The micrograph revealed the increasing average grain size with the annealing temperature. The grains of the films are spherical and uniform, and cohesion of grains is due to the magnetic attraction.
- The absorption spectrum exhibits that NiZn ferrite thin films have low absorbance in visible region and close to infrared region. The films are highly transparent in the visible range below 90%. The optical transmittance spectra of annealed thin films show a good transmission in the visible region and a sharp fall in the UV region which corresponds to the band gap.

## Acknowledgements

The authors are grateful to the Ministry of Higher Education Malaysia (MOHE) and Universiti Putra Malaysia for Research University Grant (vote number 5526200). Reprinted by permission from Springer Nature and Copyright Clearance Center, Springer, Journal of the Australian Ceramic Society, Microstructure and magnetic properties of Ni-Zn ferrite thin film synthesized using sol-gel and spin-coating technique, Yusnita, Y.; Azis, R. S.; Kanagesan, S.; and Bahmanrokh, G., licence number: 4393541427573 (2017).

## Conflict of interest

The authors declare that they have no competing interest.

## Author details

Yusnita Yusuf[1], Raba'ah Syahidah Azis[1,2]* and Muhammad Syazwan Mustaffa[2]

*Address all correspondence to: rabaah@upm.edu.my

1 Materials Synthesis and Characterization Laboratory, Institute of Advanced Technology, Universiti Putra Malaysia, Selangor, Malaysia

2 Department of Physics, Faculty of Science, Universiti Putra Malaysia, Selangor, Malaysia

## References


[1] Azim M, Atiq S, Riaz S, Naseem S. Indexing the structural parameters and investigating the magnetic properties of lanthanum doped strontium hexaferrites. IOP Conference Series: Materials Science and Engineering. 2014;**60**:1-8

[2] Rebrov EV, Gao P, Verhoeven TM, Schouten JC, Kleismit R, Turgut Z, et al. Structural and magnetic properties of sol–gel $Co_{2x}Ni_{0.5-x}$ $Zn_{0.5-x}Fe_2O_4$ thin films. Journal of Magnetism and Magnetic Materials. 2011;**323**(6):723-729

[3] Bakr NA, Salman SA, Khudhair HF. Structural and optical properties of zinc doped nickel ferrite $Ni_{(1-x)}Zn_{(x)}$ $Fe_2O_4$ thin films prepared by chemical spray pyrolysis method. Journal of Chemical, Biological and Physical Sciences. 2016;**6**(1):280-293

[4] Goldman A. Modern Ferrite Technology. 2nd ed. Pittsburgh: Springer Science and Business Media, Inc.; 2006

[5] Brinker CJ, Frye GC, Hurd AJ, Ashley CS. Fundamentals of sol-gel dip coating. Thin Solid Films. 1991;**201**(1):97-108

[6] Kayani ZN, Riaz S, Naseem S. Preparation and characterization of $SrBi_2Ta_2O_9$ (SBT) thin films. Journal of Natural Sciences and Mathematics. 2011;**49**(1):49-57

[7] Dixit G, Singh JP, Srivastava RC, Agrawal HM, Choudhary RJ, Gupta A. Annealing effect on the structural and magnetic properties of nickel ferrite thin films. Surface and Interface Analysis. 2010;**42**(3):151-156

[8] Horowitz F, Dawnay EJC, Fardad MA, Green M, Yeatman EM. Towards better control of sol-gel film processing for optical device applications. Journal of Nonlinear Optical Physics and Materials. 1997;**06**(01):1-18

[9] Brinker CJ, Schunk PR. Review of sol-gel thin film formation sol-gel dip-coating. Non-Crystalline Solids. 1992;**148**:424-436

[10] Zahi S, Daud AR, Hashim M. A comparative study of nickel-zinc ferrites by sol-gel route and solid-state reaction. Materials Chemistry and Physics. 2007;**106**(2-3):452-456

[11] Mate V, Grygar A, Kadlecova J. Sol-gel processing and magnetic properties of nickel zinc ferrite thick films. Ceramics International. 2000;**26**:507-512

[12] Gupta N, Verma A, Kashyap SC, Dube DC. Dielectric behavior of spin-deposited nanocrystalline nickel-zinc ferrite thin films processed by citrate-route. Solid State Communications. 2005;**134**(10):689-694

[13] Yan F, Zhao G, Chen Y, Song N, Zhao N, You C. One-step synthesis of $Ni_{0.5}Zn_{0.5}Fe_2O_4$ fine-patterned films via photosensitive sol-gel route. Ceramics International. 2013; **39**(7):7721-7725

[14] Bilecka I, Kubli M, Amstad E, Niederberger M. Simultaneous formation of ferrite nanocrystals and deposition of thin films via a microwave-assisted nonaqueous sol-gel process. Journal of Sol-Gel Science and Technology. 2011;**57**(3):313-322

[15] Banks. Goldman, editor. Handbook of Modern Ferromagnetic Materials. Massachusetts: Kluwer Academic Publisher; 1961

[16] Sutka A, Strikis G, Mezinskis G, Lusis A, Zavickis J, Kleperis J, et al. Properties of Ni-Zn ferrite thin films deposited using spray pyrolysis. Thin Solid Films. 2012;**526**(3):65-69

[17] Takayama A, Okuya M, Kaneko S. Spray pyrolysis deposition of NiZn ferrite thin films. Solid State Ionics. 2004;**172**(1-4):257-260

[18] Zhang Y, Zhang W, Peng C. Strong ultraviolet luminescence of ZnO thin films with nanowall-network structures. Optics Express. 2008;**16**(14):10696-10700

[19] Liu Y, Li Y, Zhang H, Chen D, Mu C. Structural and magnetic properties of NiZn-ferrite thin films prepared by radio frequency magnetron sputtering. Journal of Applied Physics. 2011;**109**(7):1-4

[20] Nie SJ, Geng H, Wang JB, Wang LS, Wang ZW, Xu R, et al. The structure and magnetic properties of NiZn-ferrite films deposited by magnetron sputtering at room temperature. Advanced Materials Research. 2013;**690-693**:1702-1706

[21] Yusnita Y, Azis RS, Kanagesan S, Bahmanrokh G. Microstructure and magnetic properties of Ni-Zn ferrite thin film synthesised using sol-gel and spin-coating technique. Journal of the Australian Ceramic Society. 2017;**53**(2):767-774

[22] Syazwan MM, Hashim M, Azis RS, Ismail I, Kanagesan S, Zulkimi MM. Magnetic phase-transition dependence on nano-to-micron grain-size microstructural changes of mechanically alloyed and sintered $Ni_{0.6}Zn_{0.4}Fe_2O_4$. Journal of Superconductivity and Novel Magnetism. 2014;**27**(6):1451-1462

[23] Klug HP, Alexander LE. X-Ray Diffraction Procedures: For Polycrystalline and Amorphous Materials. 2nd ed. New York: John Wiley & Sons; 1974

[24] Subbarao EC, Singhal LK, Merriam MF, Chakravorty O, Raghavan V. Experiments in Materials Science. New York, NY: McGraw-Hill; 1972

[25] Dixit G. Structural, magnetic and optical studies of nickel ferrite thin films. Advanced Materials Letters. 2012;**3**(1):21-28

[26] Lisfi A, Williams CM. Magnetic anisotropy and domain structure in epitaxial $CoFe_2O_4$ thin films. Journal of Applied Physics. 2003;**93**(103):8143-8145

[27] Gupta N, Verma A, Kashyap SC, Dube DC. Microstructural, dielectric and magnetic behavior of spin-deposited nanocrystalline nickel-zinc ferrite thin films for microwave applications. Journal of Magnetism and Magnetic Materials. 2007;**308**(1):137-142

[28] Idza IR, Hashim M, Rodziah N, Ismayadi I, Kanagesan S, Wan Norailiana WAR, et al. A comparative study of different sintering routes effects on evolving microstructure and B–H magnetic hysteresis in mechanically-alloyed Ni–Zn ferrite, $Ni_{0.3}Zn_{0.7}Fe_2O_4$. Journal of Materials Science: Materials in Electronics. 2015;**26**:59-65

[29] Xin Z, Xiao-Hui S, Dian-Lin Z. Thickness dependence of grain size and surface roughness for dc magnetron sputtered Au films. Chinese Physics B. 2010;**19**(8):086802

[30] Kumar N, Prasad S, Misra DS, Venkataramani N, Bohra M, Krishnan R. The influence of substrate temperature and annealing on the properties of pulsed laser-deposited YIG films on fused quartz substrate. Journal of Magnetism and Magnetic Materials. 2008;**320**(18):2233-2236

[31] Nakashima S, Fujita K, Tanaka K, Hirao K, Yamamoto T, Tanaka I. First-principles XANES simulations of spinel zinc ferrite with a disordered cation distribution. Physical Review B: Condensed Matter and Materials Physics. 2007;**75**:174443

[32] Desai M, Prasad S, Venkataramani N, Samajdar I, Nigam AK, Keller N, et al. Anomalous variation of coercivity with annealing in nanocrystalline NiZn ferrite films. Journal of Applied Physics. 2002;**91**(101):7592-7594

[33] Rodrigues D, Landgraf G, Jose F. Determining the effect of grain size and maximum induction upon coercive field of electrical steels. Journal of Magnetism and Magnetic Materials. 2011;**323**:2335-2339

[34] Bilecka I, Kubli M, Amstad E, Niederberger M. Simultaneous formation of ferrite nanocrystals and deposition of thin films via a microwave-assisted nonaqueous sol-gel process. Journal of Sol-Gel Science and Technology. 2011;**57**(3):313-322

[35] Khusayfan NM. Study of structure and electro-optical characteristics of indium tin oxide thin films. Advances in Condensed Matter Physics. 2013;**23**:1-8

[36] Yakuphanoglu F, Arslan M. The fundamental absorption edge and optical constants of some charge transfer compounds. Optical Materials. 2004;**27**(1):29-37

[37] Jain A, Sagar P, Mehra R. Changes of structural, optical and electrical properties of sol-gel derived ZnO films with their thickness. Materials Science-Poland. 2007;**25**(1):233-242

[38] Bakry A. Influence of film thickness on optical properties of hydrogenated amorphous silicon thin films. Egyptian Journal of Solids. 2008;**31**:11-22

[39] Chavan SM, Babrekar MK, More SS, Jadhav KM. Structural and optical properties of nanocrystalline Ni-Zn ferrite thin films. Journal of Alloys and Compounds. 2010;**507**(1): 21-25

[40] Joshi GP, Saxena NS, Mangal R, Mishra A, Sharma TP. Band gap determination of Ni-Zn ferrites. Bulletin of Materials Science. 2003;**26**(4):387-389

[41] Pratibha R, Godbole RV, Phase DM, Chikate RC, Sunita B. Ferrite thin films: Synthesis, characterization and gas sensing properties towards liquid petroleum gas. Materials Chemistry and Physics. 2015;**149-150**:333-338